

Comparing Taguchi-based RSM and ANN for Shredder Blade Geometrical Parameter Optimization

Trieu Khoa Nguyen*, Bach Phuong Ho Thi
Faculty of Mechanical Engineering,
Industrial University of Ho Chi Minh City, Ho Chi Minh City, VIETNAM
*nguyenkhoatrieu@iuh.edu.vn

ABSTRACT

In this study, a Taguchi-based RSM in conjunction with an ANN model was utilized to ascertain optimal geometric parameters for the shredding blade employed in a plastic bottle shredder. The shredding process is pivotal in plastic recycling, involving the reduction of waste plastic into smaller fragments to facilitate subsequent transportation and processing. Despite existing research on plastic shredders, further investigations are warranted to optimize shredding blade design. Consequently, a numerical analysis, providing an in-depth insight into understanding the shredder parameters to elucidate the influence of geometric factors was conducted. Subsequent validation was carried out using experimental designs prescribed by the Taguchi-based RSM and ANN models. Both models were then evaluated based on predictive effectiveness and error against simulation data. The predictive outcomes presented that the ANN model resulted in better prediction capacity and lower prediction error than the RSM model, $0.16197 \mu\text{m}$ and $0.15567 \mu\text{m}$, while the numerical validation value was $0.162 \mu\text{m}$. Both the original and optimal blades were fabricated and utilized for experiments, illustrating lower wear after measurement using a microscope from ICamScope®. As a result, it is evident from this inquiry that this methodology presents a viable avenue for enhancing the efficiency of plastic recycling machinery and broader industrial applications.

Keywords: Response Surface Method (RSM); Artificial Neural Network (ANN); Plastic Waste; Shredder Blade; Taguchi Method

Introduction

Along with plastic materials becoming one of the most common materials in the world, the problem of plastic waste is also becoming more and more serious. Due to the huge amount of waste generated, the long decomposition time, and the depletion of natural resources, plastic waste has now become one of the major threats to the natural environment. As a result, the demand for plastic recycling, whereby certain recyclable plastics are treated for reuse, is growing day by day. In recycling plastic waste, to improve its mobility, ease, and availability for other new plastic products, it must be separated into smaller sizes utilizing shredders. Due to the crucial of this shredding stage, there have been many studies about the design as well as fabrication of waste plastic shredders. Reddy and Raju [1] developed a shredder model that was claimed as simple, efficient, required less time, and was cost-effective when compared to the existing available model. However, the geometry of the shredding blade as well as the operating conditions of the machine have not been analysed. Ayo et al. [2] built a low-cost waste plastic shredder for small as well as medium-scale recycling plants. The shredder was assessed at 3 shredding speeds for some particle sizes. As for the works in [3]-[9], the machine has not been evaluated in terms of performance as well as the operating status of the shredding blades. Farayibi [10] also published a design for a waste plastic recycling device. In which, the chassis was simulated and analyzed utilizing SolidWorks software, while the machine's operational features have not been mentioned. Meanwhile, Jaff et al. [11] plotted and built both a shredder and an extruder for their waste plastic recycling system. However, due to limited experimental conditions, they did not have many conclusions about the operation of this system.

In plastic shredders, the shredding blade plays an important role in the shredding stage as it determines the size of the shreds as well as the life and productivity of the equipment [12]. In addition, shredding blade damage or jams are the most common errors that lead to production stoppage [13]. However, the geometrical characteristics of the shredding blade and their influence on wear and/or deformation have not been fully studied. Though in the work of Yadav et al. [13], displacement and equivalent stress investigation were performed, these outcomes were not utilized for subsequent optimization or other improvements. Similarly, using the static structural method, Sekar Ravi [14] accomplished total displacement, stress, and strain analysis. Later, the shredding blade was advanced by hardening or chromium plating to increase the mechanical characteristics while the geometry was not considered. In the same manner, Yepes et al. [15] as well as Nasr et al. [16] investigated static stress within given shredding blades with two and three cutting edges, respectively, for chopping polyethylene terephthalate (PET) waste plastic. But like other authors, they did not perform tool profile optimization. In [17], Ikpe et al. checked for the alterations of the stress allocation at some force values

via SolidWorks but did not further use this result. In [12], the authors have further studied the profile of the shredding using both simulation and experiment. They used both the Taguchi method and RSM in a combination manner. The Taguchi method and RSM are both commonly utilized to achieve optimal values of relation research factors [18]. RSM was used to prevail over the discreteness [19] of the Taguchi method as well as because of the complexity of the blade design parameters. Currently, optimization methods have been used a lot such as RSM [20]-[21], artificial neural network (ANN) [22], particle swarm optimization (PSO), genetic algorithm (GA), glowworm swarm optimization (GSO) [23] and so on. However as stated, the application of these algorithms in blade profile optimization is still lacking.

Due to this deficiency, an optimization technique utilizing Taguchi-based RSM and ANN was employed in this study. Firstly, an orthogonal array was employed to conduct the experimental design. RSM was then used to determine the optimal parameters through a self-developed Matlab script. Subsequently, the accuracy of the optimal output data was validated using the ANN-predicted model and experimental measurements. Remarkably close agreement was observed among the actual experimental results, RSM predictions, and ANN forecasts.

Description of the Shredder and its Shredding Blades

From Figure 1, it is evident that the shredder operates using a 3-phase power supply. Categorized as a single shaft type, the shredder features a shaft adorned with 14 adjustable shredding blades, as depicted in Figure 2. Furthermore, the equipment incorporates dual rows of fixed blades, comprising a combined total of 30 blades on each side. In this investigation, preliminary experiments highlighted significant deformation solely in the movable blades. Consequently, the focus of the study centered on enhancing the geometry of these movable blades. The configuration of the movable shredding blade is illustrated in Figure 2a. It was intricately fashioned in an S-shaped contour, featuring two corresponding shredding ends. Additionally, a hexagonal aperture was incorporated at the blade's center, designed for effortless attachment onto the driven shaft, obviating the necessity for a keyway. The annotations within Figure 2a depict the symbols denoting the geometric parameters harnessed for the experimental design within this study. Subsequently, the shredding blades were fabricated using laser cutting and grinding techniques, as depicted in Figure 2b.

The shredding blades were crafted from 5 mm-thick S45C steel plates, a widely adopted material selected for its cost-effectiveness, particularly well-suited for small and medium-scale production establishments. To enhance hardness, a heat treatment was administered before the final grinding process,

from 205 GPa to 460 GPa. Table 1 outlines the key attributes of this material, which are utilized for the simulations.

A 2D model of the entire blade was built to perform the simulation. The simulation analysis was performed using Comsol Multiphysics software. In this study, to discretize the simulation and computational domain, triangular elements were utilized. After being meshed, the blade model has 9892 triangular-type, 376 edge-type, and 20 vertex-type elements.

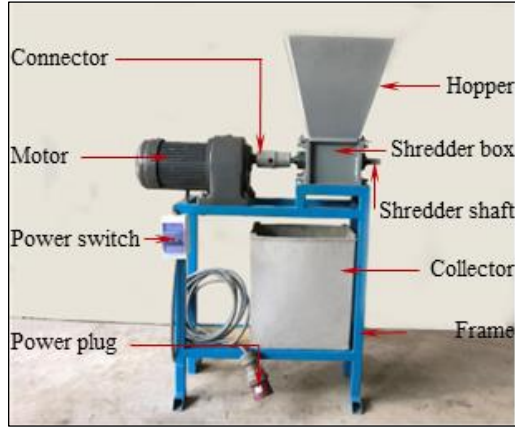


Figure 1: Details of the developed shredder in the present study

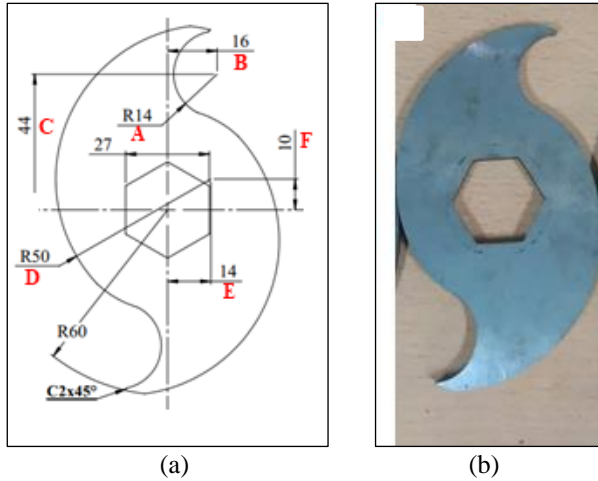


Figure 2: The shredding blade; (a) CAD design, and (b) picture of a fabricated one

Table 1: Important properties of S45C steel used for numerical analysis

Properties	Before heat treatment	After heat treatment	Unit
The density	7.78×10^3	7.78×10^3	kg/m ³
The Poisson's ratio	0.3	0.3	-
Young's modulus	205	460	GPa
The Coefficient of thermal expansion	12.5	12.5	1/K

Modelling of the Effect of the Geometrical Factor using RSM

Experimental design using Taguchi-based RSM

In the present simulation study, the response surface modelling was performed to demonstrate the mathematical relationship between the response, deformation D , and various geometrical factors. The mathematical model has been built based on a second-order polynomial as the following [24]-[25]:

$$D = \beta_0 + \sum_{i=1}^n \beta_i X_i + \sum_{i=1}^n \beta_{ii} X_i^2 + \sum_{j=1}^n \sum_{i=1}^n \beta_{ij} X_i X_j \quad (1)$$

where D is the corresponding response, $\beta_i, \beta_j, \beta_{ij}$ are the regression variables [26], n is the total number of input variables [27], and X_i, X_j are the values of the i^{th} and j^{th} geometrical parameters, correspondingly [28].

Numerous aspects could be considered in the design of the shredding blade. However, the pre-feasibility experiments highlighted that the sections most significantly affected by the shredding force and deformation were the blade's two ends. As a result, the initial optimization focus was solely on the dimensions that contribute to the shredding end. It's noteworthy that the outer diameter of the shredding blade, measuring 120 mm, remained unchanged throughout the optimization process. This decision was influenced by the continuation of prior research; the current study employed the same shredder as the preliminary experiments, except for the shredding blades.

Furthermore, three distinct levels were established for each geometric parameter based on previous preliminary tests. The specific values for each factor and the corresponding three levels utilized in this study are presented in Table 2.

Table 2: Geometrical factors and their detailed levels considered in the current investigation

Symbols	Factors	Levels			Units
		Level 1	Level 2	Level 3	
A	The diameter Ø28	27.8	28.0	28.2	mm
B	The value of coordinate x of Ø28	15.8	16.0	16.2	mm
C	The value of coordinate y of Ø28	43.8	44.0	44.2	mm
D	The diameter Ø100	99.8	100.0	100.2	mm
E	The value of coordinate x of Ø100	13.8	14.0	14.2	mm
F	The value of coordinate y of Ø100	9.8	10.0	10.2	mm

To optimize the geometry of the shredding blade, modeling the influence of its dimensions is essential to predict the response results for any arbitrary input factors. From the quantity of chosen dimensions of the shredding blade and their respective levels, a subset of the $L_{18}(3^6)$ orthogonal array (OA) was chosen as presented in Table 3. In total, 18 numerical simulations via Comsol for the shredding blades under the calculated shredding force were conducted using the dimension combinations of the OA. In this stage, 18 blade designs according to these dimension combinations were also built for simulations. The largest deformations of the blades, calculated by the numerical simulations, the mean standard deviation (MSD), and the corresponding S/N ratios were also presented in Table 3. To attain an effective shredding process, the deformation, the objective character of the investigation, should be minimized, hence the “smaller-the-better” option of the S/N ratio was used [29].

Signal-to-noise (S/N) ratio analysis

All the results of the S/N ratio analysis are presented in Table 4 and illustrated in Figure 3. As can be observed in Figure 3, as factors A , C , and E increased, the S/N ratio decreased. In other words, the deformation of the shredding ends increased. In contrast, within the study range, when factors B , D , and F increased, the deformation was predicted to decrease. By calculating the disparity between the maximum and minimum S/N ratio results of each factor, its respective contribution to the variability of the deformation result was obtained. This contribution of all factors is shown in Figure 4. Figure 4 shows that the F factor and B factor are the two factors that have the most influence on the deformation results, 28.09% and 26.54%, respectively. As shown in Figure 2a, as F (the value of coordinate y of Ø100) increased, the shredding end became thicker, resulting in reduced deformation. As factor B (the value of coordinate x of Ø28) increased, combined with the chamfer C2×45, the thickness of the shredding end also increased.

An ANOVA was also carried out as described in Table 4 to further study the contributions of the considered geometrical parameters. Just like the

S/N ratio analysis, factor *B* (the value of coordinate *x* of Ø28) and factor *F* (the value of coordinate *y* of Ø100) were considered important factors involved in reducing deformation. There was a slight difference in the contribution of factors although there was a clear qualitatively similar trend in the ANOVA and S/N ratio analysis. In addition, according to ANOVA, only four factors, *A* (diameter Ø28), *B* (the value of coordinate *x* of Ø28), *E* (the value of coordinate *x* of Ø100), and *F* (the value of coordinate *y* of Ø100) had *F* values that were greater than the corresponding $F_{(0.05,2,5)}$, thus indicating that only these geometrical parameters were statistically significant.

Table 3: OA used in the present study: Detailed values and largest deformations obtained from the numerical simulations

No.	Factors						Deformations	MSDs	S/N ratios
	<i>A</i>	<i>B</i>	<i>C</i>	<i>D</i>	<i>E</i>	<i>F</i>			
1	27.8	15.8	43.8	99.8	13.8	9.8	0.18830	0.035458	14.50286
2	27.8	16.0	44.0	100.0	14.0	10.0	0.17801	0.031689	14.99093
3	27.8	16.2	44.2	100.2	14.2	10.2	0.16526	0.027312	15.63641
4	28.0	15.8	43.8	100.0	14.0	10.2	0.17734	0.031449	15.02393
5	28.0	16.0	44.0	100.2	14.2	9.8	0.18509	0.03426	14.65219
6	28.0	16.2	44.2	99.8	13.8	10.0	0.17414	0.030326	15.18182
7	28.2	15.8	44.0	99.8	14.2	10.0	0.19171	0.036752	14.34714
8	28.2	16.0	44.2	100.0	13.8	10.2	0.17207	0.029608	15.2859
9	28.2	16.2	43.8	100.2	14.0	9.8	0.17917	0.032102	14.93467
10	27.8	15.8	44.2	100.2	14.0	10.0	0.18201	0.033129	14.79794
11	27.8	16.0	43.8	99.8	14.2	10.2	0.17490	0.030592	15.14398
12	27.8	16.2	44.0	100.0	13.8	9.8	0.17024	0.028982	15.37867
13	28.0	15.8	44.0	100.2	13.8	10.2	0.17542	0.030771	15.1186
14	28.0	16.0	44.2	99.8	14.0	9.8	0.19575	0.038318	14.16597
15	28.0	16.2	43.8	100.0	14.2	10.0	0.17729	0.031432	15.02627
16	28.2	15.8	44.2	100.0	14.2	9.8	0.20187	0.040751	13.89862
17	28.2	16.0	43.8	100.2	13.8	10.0	0.17725	0.031417	15.02832
18	28.2	16.2	44.0	99.8	14.0	10.2	0.17597	0.030964	15.09141
Sum							3.24181	0.585313	
Average							0.18010		14.90031

Table 4: Results from ANOVA

Parameters	S	f	V	F	$F_{(0.05,2,5)}$	P%	Rank
A	1.33570E-04	2	6.67850E-05	6.15036	5.78614	9.14	4
B	4.64932E-04	2	2.32466E-04	21.40824	5.78614	31.81	2
C	2.80007E-05	2	1.40004E-05	1.28932	5.78614	1.92	
D	1.15018E-04	2	5.75088E-05	5.29610	5.78614	7.87	
E	1.39479E-04	2	6.97397E-05	6.42247	5.78614	9.54	3
F	5.26260E-04	2	2.63130E-04	24.23217	5.78614	36.01	1
Error	5.42936E-04	5	1.08587E-05				
Total	1.46155E-03	17					

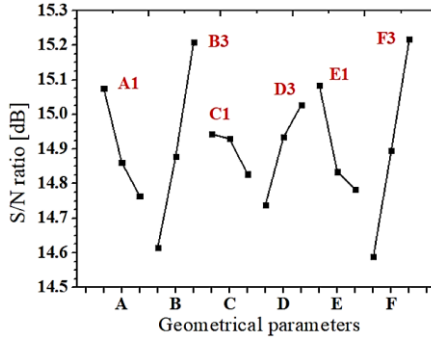


Figure 3: Results of S/N ratio showing the influences of factors on the displacement

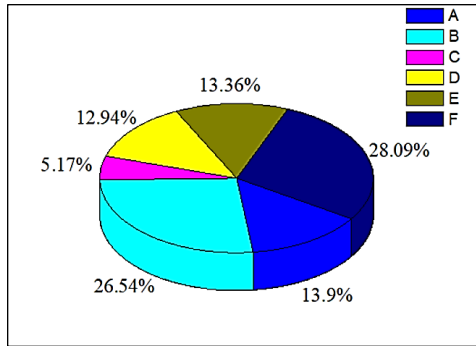


Figure 4: Contributions of factors from the S/N ratio results

Developing RSM

The Taguchi method is an effective tool that can indicate the importance of each factor as well as lead to an improved combination of dimensions involved to minimize deformation [30]. However, the improved outcomes achieved from the Taguchi method are restricted to one of the three initially designed levels for each parameter [31]. This is also evident in the results in Figure 3. Therefore, both the orthogonal array and S/N ratio from the Taguchi method were used to design the experiments and perform the preliminary analyses. RSM was used to reduce the deformation of the shedding ends when subjected to shredding force. Using the least-squares method, a second-order response model was constructed. Through the analysis of the linear regression equation, it could be seen that the coefficient R^2 was high ($R^2 = 0.943$), so the improved ability of the quadratic regression equation was not significant ($R^2 = 0.963$). Also, since there was no statistically significant correlation between the

factors, quadratic terms for the correlation and/or interaction of the two factors were not added to the quadratic regression equation.

$$\begin{aligned}
 D(\mu m) = & 252.314 - 1.567A + 4.623 \times 10^{-1}B - \\
 & 2.282C - 4.721D + 1.354E - 6.269 \times 10^{-2}F - 2.769 \times \\
 & 10^{-2}A^2 - 1.542 \times 10^{-2}B^2 + 2.601 \times 10^{-2}C^2 + 2.353 \times \\
 & 10^{-2}D^2 - 4.779 \times 10^{-2}E^2 + 1.479 \times 10^{-3}F^2
 \end{aligned}
 \tag{2}$$

From this built model, the response surfaces could be constructed to imagine the influence of the factors on the resulting deformation D . Figures 5 and 6 illustrate typical graphs of the response surfaces of this study. Figure 5 shows the effect of two factors A and B simultaneously in producing the result of deformation D (μm) with the surface plot in Figure 5a and the contour plot in Figure 5b. While Figure 6 presents the response surface created by two factors D and F with the surface plot in Figure 6a and the contour plot in Figure 6b. The lower the position of the response surface is, the smaller the resulting deformation becomes, and vice versa. The results in Figures 5 and 6 show high agreement with the initial analysis in Figure 3.

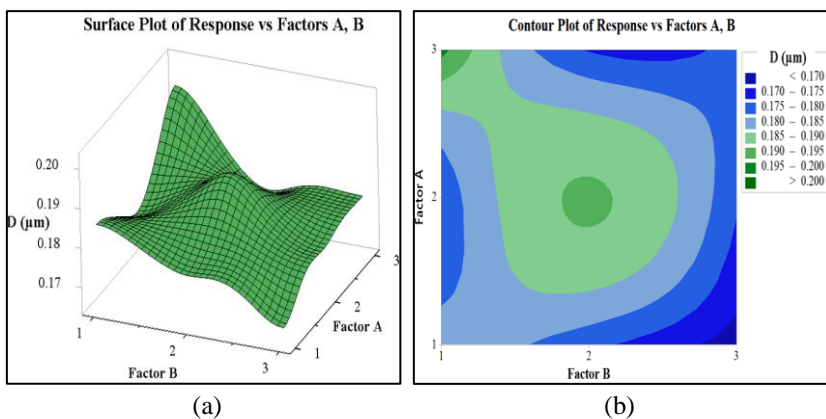


Figure 5: Response surface of the deformation D (μm) of two factors A (the diameter $\varnothing 28$) and B (the value of coordinate x of $\varnothing 28$) in (a) surface plot, and (b) contour plot

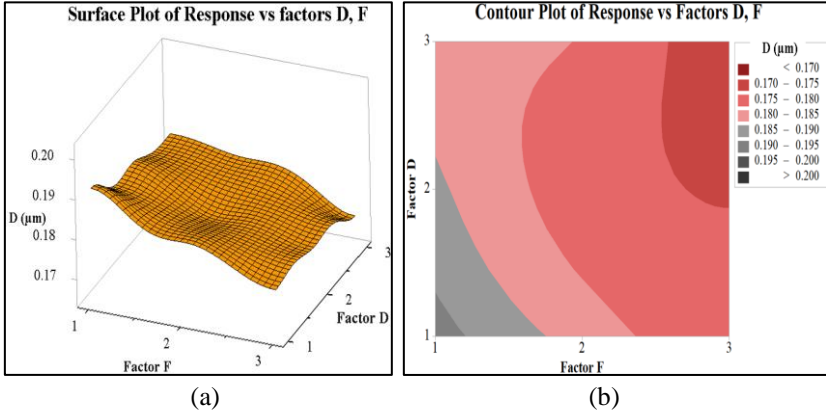


Figure 6: Response surface of the deformation D (μm) of two factors D (the diameter $\text{\O}100$) and F (the value of coordinate y of $\text{\O}100$) in (a) surface plot, and (b) contour plot

Modelling of the Effect of the Geometrical Factor using ANN

The artificial neural network (ANN) model, which deals with computation and prediction, simulates the processes of the human brain [32]. An ANN model has a specific architectural format, inspired by a biological nervous system. Any ANN model can be considered as a set of interconnected units broadly classified into 3 layers [33]. These three layers are the input layer, hidden layer, and output layer. The input factors are placed into the input layer and each node creates an output value through an activation function. The resulting outputs of the input layer are then utilized as inputs to the next hidden layer. The output of a neuron is a real value obtained by first performing a linear combination of the inputs. These inputs are the outputs of the previous layer, with their respective weights and bias, as described in the equation below [34]:

$$output = \sum_i input_i \times weight_i + bias \quad (3)$$

In this work, the model ANN consists of six neurons in one input layer and one neuron (the deformation results) in an output layer. The network is linear transfer function, ten hidden layers as shown in Figure 7. The data division was selected random (dividerand). Next, Bayesian Regularization algorithm was chosen for training. This algorithm usually needs more time, however, can give good generalizations for small datasets. According to adaptive weight minimization (regularization), training will end.

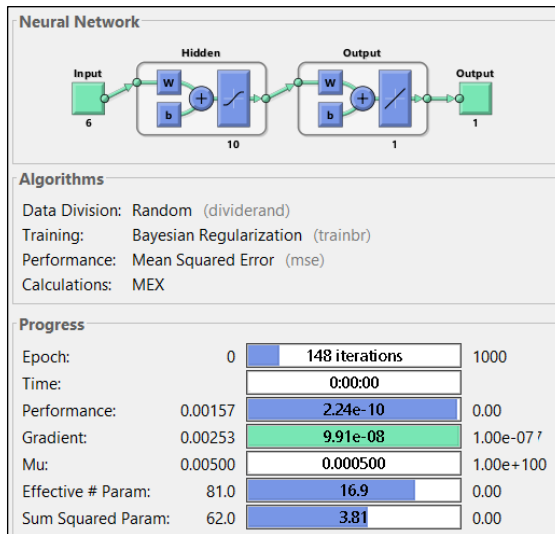


Figure 7: The ANN model for training and testing

The data in Table 3 as well as the two results from the Taguchi and RSM were used for training. The results of the ANN model are presented in Figures 8 and 9. Figure 8a demonstrates the training performance of the ANN model. Whereby, the best training performance was obtained at epoch 148 with 2.2366e-10. The performance plot in Figure 8a shows mean squared error dynamics for all datasets on a logarithmic scale. In general, the training MSE always tends to decrease, so the plot shows good training. The train line (blue line) met the best (dotted) line, which means convergence has been done. Figure 8b, the training state, illustrates some other training statistics. The gradient denotes a value of the backpropagation gradient on each iteration in a logarithmic scale. The value 9.9135e-8 means that the ANN model attained the bottom of the local minimum of the target function. The μ value obtained 5e-4 at epoch 148. During the training process, to slow the velocity of the descending so that the search value does not fly back and forth across the minimum without stopping sufficiently near it, a momentum term (μ) is added. The graph "gamk" in Figure 8b presents the average number of parameters per 148 eras that influence the precision of the outcome obtained. The value of the function "gamk" equals 16.9211 at epoch 148, which indicates that the effect of external factors, such as errors, occurred frequently [35]. The plot "ssX" presents the average sum of quadratic parameters per 148 epochs, which introduces errors in the outcome of the operation of the ANN. The outcome of the "ssX" function presents 3.8104, which is because of the minimum influence of errors on the total training outcome of the ANN. Failed

validations are iterations as validation MSE increased its value. A lot of failures denote overtraining but, in this case, it is still acceptable because the validation check equals 0 at 148 epochs as Figure 8b. It should be noted that Matlab software automatically stops training after 6 consecutive unsuccessful attempts.

According to Figures 9a and 9b, the R values for training and test are 1 and 0.99793, respectively. In the plot, the colored solid lines represent the best-fit linear regression line between outputs and targets. The R -value can be considered an indication of the correlation between the outputs and targets. The final obtained R value is 0.99792 as presented in Figure 9c. Therefore, the training data indicates a good fit. The results of the statistical analysis obtained as listed in Table 5. The training results obtained an MSE value of 2.23659e-10 and an R -square value of 0.999998.

Table 5: The outcomes of statistical analysis

	Sample	MSE	R -square
Training	14	2.23659e-10	9.99998e-1
Validation	3	0.00000e-0	0.00000e-0
Testing	3	3.70383e-6	9.97932e-1

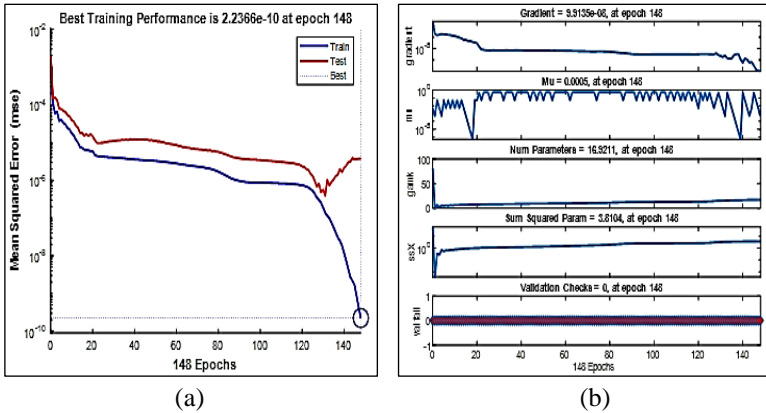


Figure 8: The training statistics, (a) performance plot, and (b) training state

Validation Using Simulation and Experiments

Validation simulation

From the S/N ratio results as in Figure 3, the minimum deformation of the shredding blade under shredding force could be attained using the combination

of $A1$, $B3$, $C1$, $D3$, $E1$, and $F3$. As mentioned earlier, considering the geometry, this combination widens the blade tip and thus minimizes distortion. An additional simulation was carried out utilizing this combination for validation, showing that the maximum blade displacement value was $0.16209 \mu\text{m}$. It can be observed that this value was smaller than the displacement results of all the cases presented in the OA, as shown in Table 3.

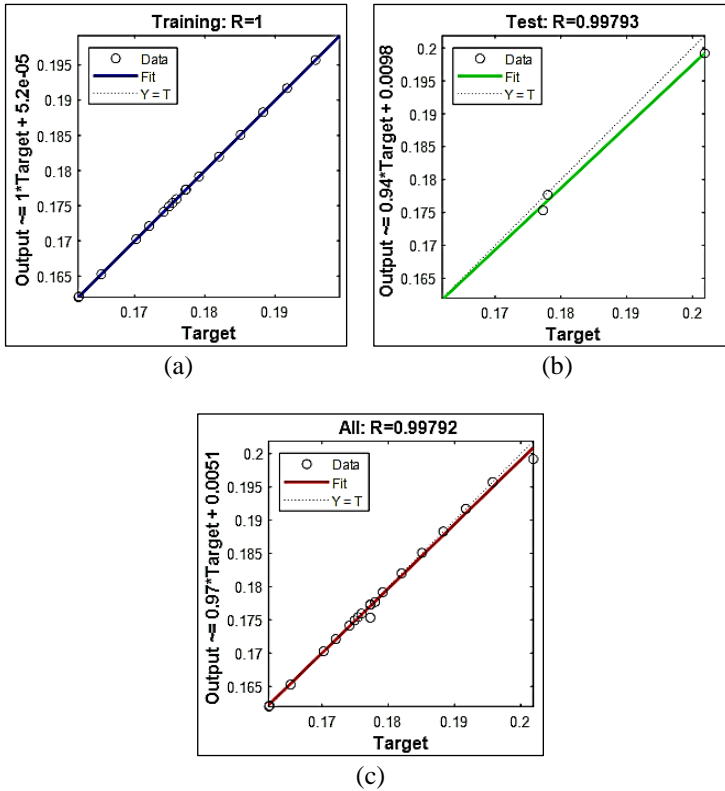


Figure 9: The neural network training regression plot, (a) training, (b) test, and (c) all

As shown in Figure 10, to verify the optimal geometrical parameters obtained utilizing RSM, a validation simulation was further accomplished. According to Table 6, the resulting maximum deformation of the shredding end was determined to be $0.16200 \mu\text{m}$, which was smaller than any other results obtained in Table 3. Also in Table 6, the predictive value of the ANN method is $0.16197 \mu\text{m}$, closer to the simulated value ($0.16200 \mu\text{m}$) than the predicted result from the RSM model, $0.15567 \mu\text{m}$. Next, the prediction results

of the two models are presented and analyzed in Figure 11. Figure 11a shows the simulation results of the shredding end deformation under different geometric conditions and the corresponding prediction results of the two RSM and ANN models. The results from the ANN model closely followed the simulation results more than the results from the RSM model. These errors are presented in more detail in Figure 11b. These results clearly show that, when used, the ANN model provides more accurate predictions than the RSM model. The prediction results from ANN are slightly more accurate than those from RSM, as shown in Figure 11. The maximum error is 0.0029 if compared with 0.0063. This accuracy may not be much in this industrial application. In industrial practice, one must balance implementation costs, software installation costs, as well as implementation time and achieve efficiency. Therefore, people usually do not need overly complicated measures. However, in the current study, it proves the correctness of the method applied. From there, this method can be considered for applications in research/production where high accuracy is required.

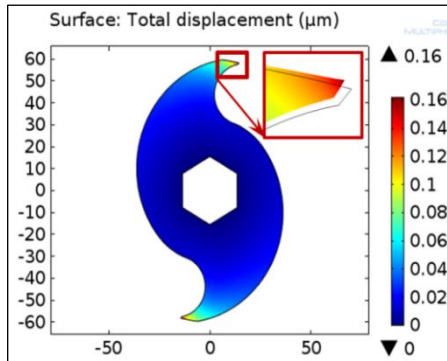


Figure 10: Simulation result using the optimized geometrical factors from RSM

Table 6: Recommended geometrical parameters

Symbols	Geometrical parameters	Taguchi	RSM	ANN
A	The diameter Ø28 (mm)	27.8	27.8	27.8
B	The value of coordinate x of Ø28 (mm)	16.2	16.2	16.2
C	The value of coordinate y of Ø28 (mm)	43.8	43.865	43.865
D	The diameter Ø100 (mm)	100.2	100.2	100.2
E	The value of coordinate x of Ø100 (mm)	13.8	13.8	13.8
F	The value of coordinate y of Ø100 (mm)	10.2	10.2	10.2
	Predicted values	N/A	0.15567	0.16197
	Numerical validations	0.16209	0.16200	0.16200

Validation experiments

The initial set of shredding blades employed in the shredder exhibited significant deformation after running for five hours, as depicted in Figure 12. Consequently, there arose a necessity to enhance the profile of the shredding blades. Following the optimization of the shredding blades through simulation, they were manufactured and subjected to testing. Both the Taguchi and RSM-optimized shredding blades were evaluated concurrently to ensure a fair and equitable assessment.

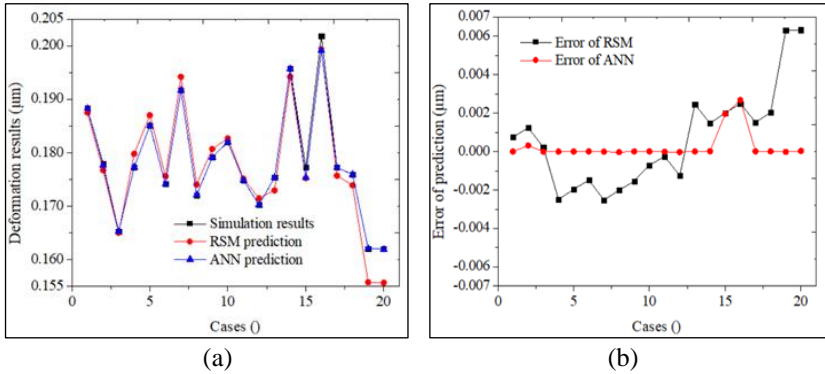


Figure 11: Simulation and prediction results from RSM and ANN models, (a) deformation results, and (b) error of prediction

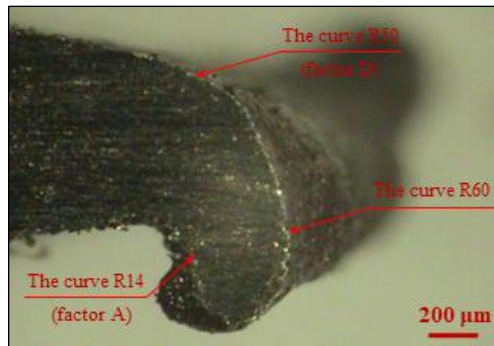


Figure 12: Illustration of the shredding blade before being optimized via Icamscope®

The two types of optimized blades were then microscopically measured after approximately 5 hours of continuous work. Figures 13a and b show the respective dimensions of the blade's tip according to the Taguchi and RSM

methods before the experiment. The sizes were $63\ \mu\text{m}$ and $62\ \mu\text{m}$, respectively; therefore, they could be considered equivalent. Next, Figures 14b and b show their dimensions after about 5 hours of continuous work. The radius of the cutting tip of the blade from the Taguchi method was enlarged to $88\ \mu\text{m}$ whereas the tip from the RSM was increased to $71\ \mu\text{m}$ only. These results validated an improvement of the optimization process by experiments.

It was thus validated, both numerically as well as experimentally, that the proposed Taguchi-based RSM method was effective enough to triumph the limitations of the Taguchi method as a discrete optimization method. In addition, the ANN model could be used to predict the deformation of the shredding blade more accurately.

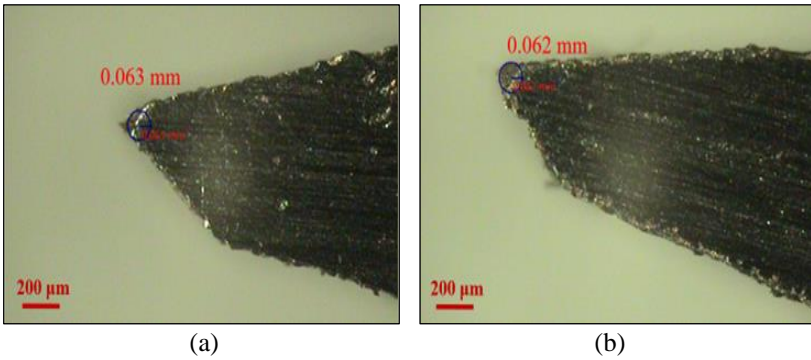


Figure 13: Illustration of the shredding blade before working for about 5 hours via ICamScope®; (a) from the Taguchi method, and (b) from RSM

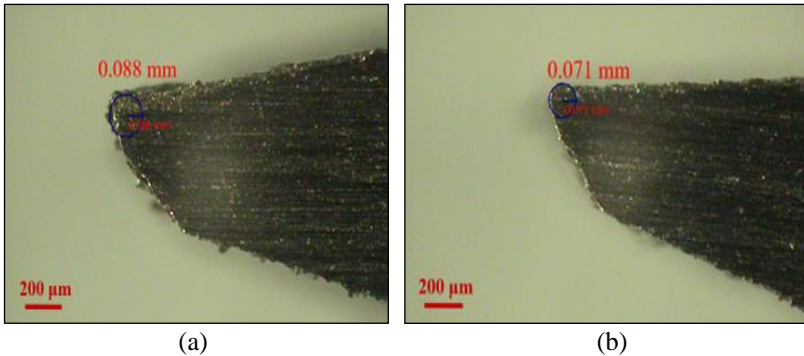


Figure 14: Illustration of the shredding blade after working for about 5 hours via ICamScope® (a) from the Taguchi method, and (b) from RSM

Conclusions

In the present work, an optimization method using both RSM and ANN based on the Taguchi platform was used to study the influence of geometrical factors of the shredding end of a waste plastic shredder on its deformation under shredding force and to determine the optimal combination for the minimum deformation. This method utilized a combination of DOE using orthogonal arrays and ANOVA of the Taguchi method with response surface analysis RSM and ANN prediction model. In numerical simulations of the shredding blade, six geometrical elements constituting the shredding end, which is mainly subjected to the shredding force, were considered. Applying the S/N ratio analysis as well as ANOVA based on the Taguchi method with $L_{18} (3^6)$ OA, the two most important factors for minimizing displacement of the shredding end were identified. The RSM and a self-developed Matlab script were used to determine the optimal parameters and the ANN model was used to accurately predict the deformation results. After using ANN, the error was improved from 0.0063 to 0.0029. Or, while the S/N ratio was utilized to identify the important factors, the RSM and/or ANN method was used to fine-tune these factors. These results were then experimentally validated by measurements using the microscope of IcamScope®. Hence, it can be deduced with clarity from this investigation that the application of this approach presents a viable option for enhancing the operational efficiency of plastic recycling machinery. Moreover, the efficacy of the method proposed herein is anticipated to bridge the existing disparity between academic research and practical industrial manufacturing endeavours.

Contributions of Authors

All authors reviewed and approved the final version of this work.

Funding

This work received no specific grant from any funding agency.

Conflict of Interests

All authors declare that they have no conflicts of interest

Acknowledgment

The measurement process using the ICamScope® microscope was carried out at the Advanced Design & Manufacturing Process (ADMP) Laboratory, Ho Chi Minh City University of Technology.

References

- [1] S. Reddy and T. Raju, "Design and Development of mini plastic shredder machine," *IOP Conference Series: Materials Science and Engineering*, vol. 455, pp. 1-7, 2018.
- [2] A. Ayo, O. J. Olukunle, and D. J. Adelabu, "Development of a waste plastic shredding machine," *International Journal of Waste Resources*, vol. 7, pp. 1-4, 2017.
- [3] Y. M. Sonkhaskar, A. Sahu, A. Choubey, A. Singh, and R. Singhal, "Design and development of a plastic bottle crusher," *International Journal of Engineering Research & Technology*, vol. 3, pp. 297-300, 2014.
- [4] D. Atadious and O. Joel, "Design and construction of a plastic shredder machine for recycling and management of plastic wastes," *International Journal of Scientific and Engineering Research*, vol. 9, pp. 1379-1385, 2018.
- [5] S.B.Satish, J. S. Sandeep, B.Sreehari, and Y. M. Sonkhaskar, "Designing of a Portable Bottle Crushing Machine," *International Journal for Scientific Research & Development*, vol. 4, pp. 891-893, 2016.
- [6] M. I. Faiyyaj, M. R. Pradip, B. J. Dhanaji, D. P. Chandrashekhar, and J. S. Shivaji, "Design and development of plastic shredding machine," *International Journal of Engineering Technology Science and Research*, vol. 4, pp. 733-737, 2017.
- [7] T. A. Olukunle, "Design Consideration of a Plastic Shredder in Recycling Processes," *International Journal of Industrial and Manufacturing Engineering*, vol. 10, pp. 1838-1841, 2016.
- [8] N. D. Jadhav, A. Patil, H. Lokhande, and D. Turambe, "Development of plastic bottle shredding machine," *International Journal of Waste Resources*, vol. 8, pp. 1-4, 2018.
- [9] A. Tegegne, A. Tsegaye, E. Ambaye, and R. Mebrhatu, "Development of dual shaft multi blade waste plastic shredder for recycling purpose," *International Journal of Research and Scientific Innovation*, vol. 6, pp. 49-55, 2019.
- [10] P. K. Farayibi, "Finite element analysis of plastic recycling machine designed for production of thin filament coil," *Nigerian Journal of Technology*, vol. 36, pp. 411-420, 2017.

- [11] J. M. A. Jaff, D. A. Abdulrahman, Z. O. Ali, K. O. Ali, and M. H. Hassan, "Design and fabrication recycling of plastic system," *International Journal of Scientific & Engineering Research*, vol. 7, pp. 1471–1486, 2016.
- [12] T. K. Nguyen, M. Q. Chau, T.-C. Do, and A.-D. Pham, "Characterization of geometrical parameters of plastic bottle shredder blade utilizing a two-step optimization method," *Archive of Mechanical Engineering*, vol. 68, pp. 253–269, 2021.
- [13] S. Yadav, S. Thite, N. Mandhare, A. Pachupate, and A. Manedeshmukh, "Design and development of plastic shredding machine," *Journal of Applied Science and Computations*, vol. 4, pp. 21–25, 2019.
- [14] L. R. Sekar, and S. Vinoth Kumar, "Utilization of upgraded shredder blade and recycling the waste plastic and rubber tyre," in *International Journal of Science and Research*, vol. 7, no. 9, pp. 1-6, 2018.
- [15] C. P. Yepes, P. R. M. Angel, and P. G. Jose, "Analysis by means of the finite element method of the blades of a PET shredder machine with variation of material and geometry," *Contemporary Engineering Sciences*, vol. 11, pp. 4113–4120, 2018.
- [16] M. F. Nasr and K. A. Yehia, "Stress analysis of a shredder blade for cutting waste plastics," *Journal of International Society for Science and Engineering*, vol. 1, pp. 9–12, 2019.
- [17] A. Ikpe and O. Ikechukwu, "Design of used PET bottles crushing machine for small scale industrial applications," *International Journal of Engineering Technologies*, vol. 3, pp. 157–168, 2017.
- [18] T. K. Nguyen, C. J. Hwang, and B.-K. Lee, "Numerical investigation of warpage in insert injection-molded lightweight hybrid products," *International Journal of Precision Engineering and Manufacturing*, vol. 18, pp. 187–195, 2017.
- [19] T. K. Nguyen and B.-K. Lee, "Investigation of processing parameters in micro-thermoforming of micro-structured polystyrene film," *Journal of Mechanical Science and Technology*, vol. 33, pp. 5669–5675, 2019.
- [20] A. V. U. K. Kandala, D. G. Solomon, and J. J. Arulraj, "Advantages of taguchi method compared to response surface methodology for achieving the best surface finish in wire electrical discharge machining (WEDM)," *Journal of Mechanical Engineering*, vol. 19, pp. 185–199, 2022.
- [21] N. A. Yaacob, A. Khasri, N. H. M. Salleh, and M. J. M. Ridzuan, "Statistical Optimization of AC/TiO₂-Cu Composite via Response Surface Methodology (RSM)," *Journal of Mechanical Engineering*, vol. SI 11, pp. 199–209, 2022.
- [22] B. B. Pradhan and B. Bhattacharyya, "Modelling of micro-electrodischarge machining during machining of titanium alloy Ti—6Al—4V using response surface methodology and artificial neural network algorithm," *Proceedings of the Institution of Mechanical*

- Engineers, Part B: Journal of Engineering Manufacture*, vol. 223, pp. 683–693, 2009.
- [23] M. H. M. Hazwan, S. Z. Abd. Rahim, S. Sharif, M. N. Mat Saad, and M. Rashidi, “Warping optimisation on the moulded part using response surface methodology (RSM) and Glowworm Swarm Optimisation (GSO),” *MATEC Web of Conferences*, vol. 97, p. 01105, 2017.
- [24] Asif Afzal, Abdul Aabid, Ambareen Khan, Sher Afghan Khan, Upendra Rajak, Tikendra Nath Verma, Rahul Kumar, “Response surface analysis, clustering, and random forest regression of pressure in suddenly expanded high-speed aerodynamic flows”, *Aerospace Science and Technology*, vol. 107, p. 106318, 2020.
- [25] I. Tharazi, A. B. Sulong, F. M. Salleh, A. H. Abdullah, and N. F. Ismail, “Application of response surface methodology for parameters optimization in hot pressing kenaf reinforced biocomposites,” *Journal of Mechanical Engineering*, vol. 17, pp. 131–144, 2020.
- [26] A. Afzal, I. Mokashi, S. A. Khan, N. A. Abdullah, M. H. Azami, “Optimization and analysis of maximum temperature in a battery pack affected by low to high Prandtl number coolants using response surface methodology and particle swarm optimization algorithm”, *Numerical Heat Transfer, Part A: Applications*, vol. 79, pp. 406-435, 2021.
- [27] B.N. Sharath, C.V. Venkatesh, A. Afzal, N. Aslfattahi, A. Aabid, M. Baig, B. Saleh, “Multi ceramic particles inclusion in the aluminium matrix and wear characterization through experimental and response surface-artificial neural networks,” *Materials*, vol. 14, pp. 1-24, 2021.
- [28] A. Afzal, R. G. Roy, C. P. Koshy, Y. Alex, M. Abbas, E. Cuce, R. K. A. Razak, S. Shaik, C. A. Saleel, “Characterization of biodiesel based on plastic pyrolysis oil (PPO) and coconut oil: Performance and emission analysis using RSM-ANN approach”, *Sustainable Energy Technologies and Assessments*, vol. 56, p. 103046, 2023.
- [29] N. F. Omar, N. A. Wahab, I. N. Ahmad, and N. Sulong, “Optimising sintering parameters on the characteristic of injection moulded 316L stainless steel utilising water soluble system,” *Journal of Mechanical Engineering*, vol. SI 8, pp. 48–64, 2019.
- [30] C. Padhy and P. Singh, “Optimization of machining parameters using taguchi coupled grey relational approach while turning Inconel 625,” *Journal of Mechanical Engineering*, vol. 18, pp. 161–176, 2021.
- [31] T.K. Nguyen, K. Chau Duc & A-D. Pham, “Characterization of an FDM-3D printed moldcore in a thermoforming process using taguchi in conjunction with lumped-capacitance method,” *Arabian Journal for Science and Engineering*, vol. 48, pp. 11989-12000, 2023.
- [32] S. Walczak and N. Cerpa, “Artificial neural networks,” in *Encyclopedia of Physical Science and Technology*, 3rd ed. Academic Press, New York, 2003, pp. 631–645.

- [33] A. P. S. V. R. Subrahmanyam, P. S. Rao, and K. S. Prasad, "Enhancement of surface quality of dmls aluminium alloy using rsm optimization and ANN modelling," *Journal of Mechanical Engineering*, vol. 18, pp. 37–56, 2021.
- [34] F. Altenberger and C. Lenz, "A non-technical survey on deep convolutional neural network architectures," *ArXiv*, vol. abs/1803.02129, 2018.
- [35] E. A. Muravyova and R. F. Gabitov, "Development of the intellectual complex for parallel work of steam boilers," *Journal of Physics: Conference Series*, vol. 1889, no. 2, pp. 1-9, 2021.